Tonal Noise Control using Rotor Phase Synchronization

Noah H. Schiller
Research Scientist
NASA Langley Research Center
Hampton, VA, USA

Kyle A. Pascioni
Research Aerospace Engineer
NASA Langley Research Center
Hampton, VA, USA

Nikolas S. Zawodny
Research Aerospace Engineer
NASA Langley Research Center
Hampton, VA, USA

ABSTRACT

The purpose of this study is to determine if phase synchronization can be used to reduce the net radiated sound power from two rotors. Phase synchronization implies that the rotors have the same rotational speed with a fixed relative azimuthal blade position, or phase. The concept is evaluated both experimentally and numerically. Measurements of source directivity and thrust are initially compared with predictions to confirm that the model accurately captures the relevant trends. The model is then used to explore the design space and identify relevant parameters. Both experimental and numerical results show that the radiated sound power at the blade passage frequency can be reduced by appropriately controlling the relative azimuthal phase of the rotors. Vehicle level predictions are also provided for a notional octocopter, comparing two different modes of operation. Predictions show that phase synchronization can be used to achieve a 4-5 dB reduction of the sound pressure level at the blade passage frequency nearly everywhere on the ground plane beneath the vehicle.

NOMENCLATURE

k	Acoustic wavenumber, [rad/m]
c	Sound speed, [m/s]
d	Hub to hub separation distance, [m]
A	Element area, [m^2]
h	Element height, [m]
i	Measurement grid index
I	Acoustic intensity, [W/m^2]
p	Acoustic pressure, [Pa]
PWL	Sound power, [dB re. 10^{-12} W]
r	Radial offset from the source, [m]
R	Microphone radial offset used in tests, [m]
SPL	Sound pressure level, [dB re. 20x10^{-6} Pa]
ΔPWL	Normalized sound power, [dB]
ϕ	Observer azimuthal angle, [deg.]
ψ_r	Relative phase angle, [deg.]
ρ	Density, [kg/m^3]
θ	Observer elevation angle, [deg.]

INTRODUCTION

Advanced vertical takeoff and landing vehicles are being developed to perform new missions in urban environments. Since these vehicles will be operating near people, community noise concerns could ultimately limit vehicle acceptability. Therefore, noise control strategies need to be considered during the design process. In many cases, appropriate strategies will depend on the vehicle type. While there are a wide variety of aircraft concepts being considered, a number of proposed vehicles include multiple, sometimes many, rotors (Ref. 1).While there are tradeoffs, increasing the rotor count can provide redundancy and mitigate the consequences of a single engine failure. Redundancy also provides operational flexibility, which can be used to reduce certain aspects of vehicle noise. This paper considers the potential acoustic benefit of using pairs of matched rotors. In this context, matched implies that the rotors have the same nominal blade shape, collective control inputs (if the rotors are not fixed-pitch), and rotational speed. The inflow is also assumed to be similar. In other words, the two rotors are assumed to be acoustically equivalent. Using pairs of rotors with matched collective inputs and rotational speed will eliminate degrees of freedom. Therefore, this approach is not applicable to all multicopter configurations, or even flight modes, but could be viable for a subset of vehicles with sufficient redundancy.

Related studies have explored the possibility of using propeller phase control to modify the acoustic characteristics of a vehicle during flight (Refs. 2-4). Phase control, or phase synchronization, implies that the propulsors are synchronized (i.e., rotating at equivalent rates) and relies on changes to the relative azimuthal blade position, or phase, to minimize the blade passage frequency noise radiated in specific directions. Attenuation, however, is typically achieved in exchange for amplification in other directions. While this is a useful capability for certain missions, it may not be appropriate for others. For instance, if the vehicle is flying over a heavily

---

populated area, it may be undesirable to have amplification in any direction. The purpose of this study is to determine if a net acoustic benefit, averaged over all directions, can be achieved by controlling the relative phase of pairs of matched rotors. As with previous studies, this effort is focused exclusively on the steady tonal noise produced at the blade passage frequency, which can be dominant in some flight conditions, particularly if the rotors are lightly loaded.

This study includes an experimental and numerical assessment of the proposed two rotor system. Therefore, the paper begins with descriptions of the test setup and numerical model. Results are then presented, starting with measured spectra, mean thrust, and source directivity. Numerical results are presented to justify a farfield approximation that is used to calculate radiated sound power from pressure measurements. Predicted and measured sound power are then compared. A physical explanation is proposed, and finally the potential vehicle level benefit is presented for a notional vehicle.

METHODOLOGY

Both the experimental and numerical procedures used to conduct the study are described in this section.

Experimental

EXPERIMENTAL SETUP

Tests were performed on the dual rotor assembly pictured in Figure 1. Each rotor has two CF125 blades, distributed by KDE Direct, with an overall diameter of 317 mm. The hub to hub separation is 400 mm, which gives a tip to tip clearance of 83 mm. Each hub is attached to a short shaft, which increases the clearance between the rotors and support arm. Specifically, the tips of the rotors are 59 mm above a 13 mm diameter support arm. While the presence of the airframe will increase the harmonic content relative to an isolated rotor, the change at the blade passage frequency is expected to be negligible (Ref. 5). Both rotor shafts are connected to a single brushless DC electric motor by timing belts and pulleys, which synchronize the rotation rate and fix the relative phase offset of the two rotors. The relative size of the pulleys results in a 6:1 speed ratio, such that the motor, a Scorpion HKII-2221-10, spins 6 times faster than the rotors. While synchronization is achieved mechanically in this case, phase control could also be achieved with a compact microcontroller coupled to a pair of motor speed controllers (Ref. 6).

An optical tachometer was used to measure the rotation rate of the motor, which was set to 30,600 RPM for all tests described in this paper. This corresponds to a rotor rotation rate of 5,100 RPM and a blade passage frequency of 170 Hz. The rotation direction of each rotor was determined by the twist in the drive belts extending from the center shaft to the rotor shaft. A one-quarter twist in one direction produced clockwise rotation of the rotor shaft, while a one-quarter twist in the other direction generated counterclockwise rotation.

For all tests, nominally identical clockwise and counterclockwise blade sets were used, as needed.

Figure 1. Dual rotor assembly from the front and side.

The dual rotor assembly was installed on top of a JR3 30E15A4 multiaxis load cell used to measure thrust. The entire assembly was mounted on a rotation stage on top of a test stand located in the center of the Structural Acoustic Loads and Transmission (SALT) anechoic facility at the NASA Langley Research Center. The interior dimensions of the chamber are 9.63 m by 7.65 m by 4.57 m (measured from wedge tip to wedge tip). The wedges create a nearly free-field acoustic environment down to approximately 100 Hz (Ref. 7). Five 6.35 mm diameter free-field microphones were positioned at a common radial distance, 1.9 m, from the center of the test article. All microphones were arranged at a common azimuthal angle, but at different elevation angles of 0°, -11.25°, -22.5°, -33.75° and -45°, denoted by M1-M5 in Figure 2, respectively.
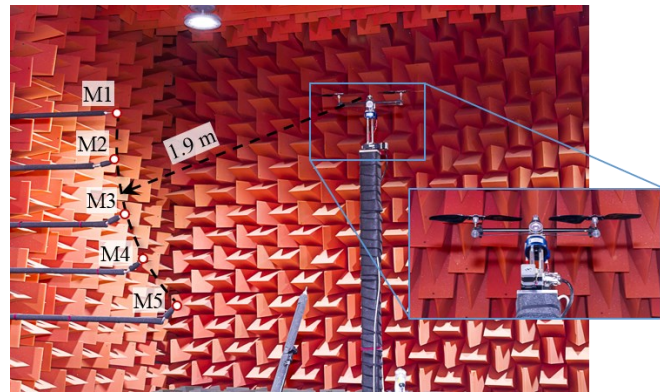

Figure 2. Test setup in the NASA Langley Structural Acoustic Loads and Transmission (SALT) anechoic chamber.
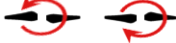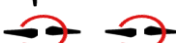
While the microphone array was stationary, the dual rotor assembly was mounted on a rotation stage that could be used to rotate the assembly relative to the microphones to capture the source directivity. In total, tests were performed at 31 different azimuthal angles spanning 348.75° in 11.25° steps. Data acquired with the microphones directly in front of the assembly, such that the rotors were equidistant from the microphones, corresponded to an azimuthal angle of 0°. As the assembly rotated clockwise, from above, the angle increased. For reference, Figure 2 shows the microphone array at an azimuthal angle of 270°.

The acquisition was typically started with the rotors static. The motor was brought up to speed, reaching steady-state after 5-10 seconds. A total of 15 seconds of data were

collected at a sample rate of 51.2 kHz. The motor was then stopped before the assembly was rotated to the next azimuthal angle. The typical down time between runs was 2 minutes, which was sufficient to allow the air in the chamber to settle before the next run. While flow recirculation in a closed chamber can corrupt acoustic and load measurements (Ref. 8), the size of the chamber, modest rotation rate, and relatively short time duration of each run mitigated this risk.

The test matrix included six different rotor configurations, as shown in Table 1. The first test was performed with only one rotor installed. For this particular test, measurements were collected at a subset of the full azimuthal angles since a single rotor should have a uniform azimuthal directivity. The remaining tests were conducted with both rotors installed and measurements were collected over the full range of azimuthal angles. The tests labeled counterrotating indicate that the two rotors were spinning in opposite directions, while corotating implies that the rotation direction was the same. Different relative phase offsets, ψ_r, were also considered, as indicated in Table 1. Note that the graphical representations in the table depict the rotation direction of each rotor as viewed from below.

Table 1. Test matrix.

Number of rotors	Relative rotation direction	Relative phase, ψ_r	Graphical representation
1	n/a	n/a	
2	counterrotating	0°	
2	counterrotating	90°	
2	corotating	0°	
2	corotating	45°	
2	corotating	90°	

POST-PROCESSING

Following the test, pressure time histories were available at a large number of discrete points on a hemisphere around the dual rotor assembly. Acoustic spectra were computed using a fast Fourier Transform with a Hanning window, 75% overlap, and a frequency resolution of 5 Hz. Only the last two seconds of data were used, to allow the system to reach steady state. Since the study is focused on the steady tonal noise produced at the blade passage frequency, all spectral energy within 10 Hz of the peak at the blade passage frequency (i.e., 170 Hz) was combined on a pressure squared basis. Neighboring spectral bins were included to account for small variations in the rotational rate during and between tests. While the response at the blade passage frequency is sufficient to validate the numerical model, the experimental

data can also be used to directly quantify the sound power radiated through the measurement grid. This calculation, however, requires the use of a farfield approximation, which is assessed elsewhere in this paper. If the approximation holds, then intensity can be calculated from the pressure measurements. Specifically, the intensity normal to the measurement surface can be calculated as

$$I_i = p_i^2/(\rho c) \tag{1}$$

where p_i^2 is the mean square pressure, within 10 Hz of the blade passage frequency, at the ith measurement location. The hemispherical surface defined by the measurement grid, depicted in Figure 3, can then be discretized and the area associated with each element can be calculated as

$$A_i = \frac{2\pi R h_i}{32} \tag{2}$$

where R is the separation distance from the center of the assembly to the measurement location, and h_i is the height of each element. The quantity is divided by 32 to account for the discretization in the azimuthal direction. The height of each element can be computed as

$$h_i = R\sin(\theta_i + 5.625°) - R\sin(\theta_i - 5.625°) \tag{3}$$

where θ_i is the elevation angle. The overall power radiated through the measurement grid, PWL, can then be found by adding the power radiated through each element

$$PWL = \sum_{i=1}^{155} I_i A_i \tag{4}$$

Note that while a full grid contains 160 (i.e., 32 x 5) elements, measurements were only acquired at 31 of the possible 32 azimuthal angles due to limitations associated with the rotation stage. Therefore, the sound power calculation accounts for all energy radiated through a hemispherical section that is missing one 11.25° azimuthal slice.
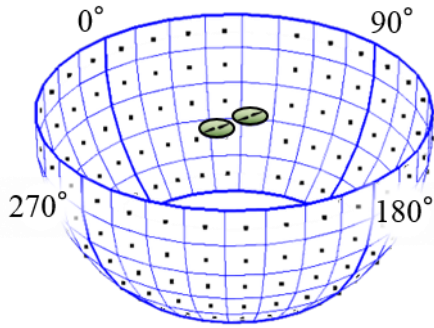
Figure 3. Measurement grid surrounding the dual rotor system. The relative location of the rotors is indicated by the green disks, the measurement locations are shown in black, and the blue grid represents the discretized surface used in the radiated power calculation.

Recall that measurements were collected at a subset of the azimuthal angles during the single rotor test. Therefore, the data from that particular test were processed differently. Since the directivity of a single isolated rotor is uniform about the azimuth, a single spatially averaged p^2 value was calculated for each elevation angle based on the available measurements. The averaged p^2 values for each elevation angle were then used to populate a larger matrix consistent with the dense measurement grid. The data from all six tests could then be processed in the same way, using Equations 1-4, to calculate the radiated sound power through the same hemispherical section.

Numerical

NOISE PREDICTION METHOD

Predictions were generated for each pair of phase synchronized rotors by combining predictions for isolated rotors with the appropriate rotation direction and relative azimuthal phase. The isolated rotor predictions were generated using the Propeller Analysis System (PAS) module (Ref. 9) within the NASA Aircraft NOise Prediction Program (ANOPP) (Ref. 10). PAS is a comprehensive propeller prediction program that computes the potential flow around a set of 2-D blade sections and models boundary layer parameters on each section, generating airfoil tables, which are functions of lift coefficient, angle of attack, and Mach number. Using this information, surface pressure, propeller performance, induced flow, and acoustic pressure time histories at specified observer locations can be calculated. Since the prediction process used in this paper mimics the procedure described in previous references, some details have been omitted. The reader is referred to (Refs. 2-4) for a more complete explanation of the prediction process.

PAS uses blade element momentum theory to calculate the steady loading on the surface of the blades based on the blade geometry, rotation rate, and in-flow velocity. The blade geometry was defined in terms of airfoil section coordinates estimated from measurements collected on one of the CF125 blades. The shape of the airfoil was assumed constant along the blade, but the chord and twist angle varied significantly. To estimate these, measurements were taken at 25 radial locations along the blade. The airfoil shape was found by scanning and discretizing a single cross-sectional cut of the blade near midspan. The airfoil section coordinates were then calculated for each radial station by appropriately scaling and rotating the midspan shape. The other inputs to the code include rotation rate, which was set at 5,100 RPM, and in-flow velocity. PAS is a propeller analysis code, which requires a nonzero inflow velocity. Therefore, hover was approximated with an inflow velocity of 1.5 m/s, which has worked well in previous studies (Refs. 3, 11).

Based on the blade geometry, motion, and surface pressure, the tonal noise (steady loading and thickness noise) was then predicted on either a hemisphere, or sphere, surrounding each isolated rotor using the F1A formulation (Ref. 12) of the Ffowcs-Williams Hawkings equation. Once the source hemisphere or sphere was defined, the acoustic data were then propagated, accounting for time delay and spherical spreading, to the set of observer locations where the total response was found by adding the acoustic pressure from each rotor.

This two-step approach is efficient for many situations. Once the source is defined, the response at any number of observer locations can be calculated without the need to repeat the source calculation. However, it is not applicable for acoustic predictions in the nearfield due to the simplified way sound is propagated. Therefore, the assessment of the farfield approximation, described later in this paper, was performed using a single step process. Specifically, the rotors were modeled in isolation, and predictions, which include nearfield terms, were generated along a line extending away from the center of the assembly. The acoustic pressure due to each rotor was then combined at each point along the line, eliminating the need for the propagation step.

VEHICLE LEVEL PREDICTION

There are several vertical lift vehicles being evaluated by the community which include multiple rotors with sufficient redundancy to utilize phase control. One of the simplest configurations to evaluate is an octocopter. In this case, pairs of rotors could be synchronized without sacrificing vehicle performance. The vehicle level assessment was therefore performed on a relatively small octocopter in hover, with the rotor layout shown in Figure 4. The nominal rotor rotation rate was assumed to be 5,100 RPM to match the tests. The size and separation distance between rotors were also selected to match the test hardware, resulting in a vehicle with an overall diameter of 1.02 m, tip to tip.

Vehicle level predictions were generated using the two-step approach previously described. Two different vehicle configurations were considered. In one case, all eight rotors were assumed to be independent. A second configuration was also considered with neighboring pairs of rotors, identified in Figure 4 by color, synchronized and phased appropriately to

4

minimize noise at the blade passage frequency. For the reference case, the rotors were assumed to have the same nominal rotation rate, but would be controlled independently and therefore would not have a stable phase relationship. Since phase would be arbitrary, pressure was combined on a linear energy (i.e., pressure squared) basis at each observer location. In contrast, with the rotors synchronized, pairs of sources would be coherent with a stable phase relationship. In this case, the pressure was combined at the observer locations to capture the resulting interference pattern due to the phase offset. For this type of vehicle, however, it would only be possible to synchronize individual pairs of rotors and still maintain stable flight. Therefore, the sound produced by each pair needed to be combined at the observer locations on a pressure squared basis.
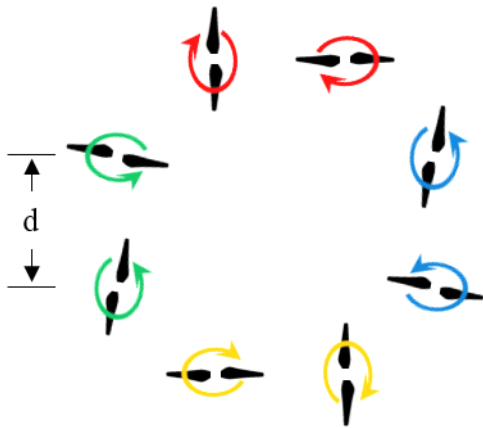

Figure 4. Assumed rotor layout for notional octocopter with synchronized pairs of rotors.

RESULTS AND DISCUSSION

This section presents both the experimental and numerical results, including spectra, directivity, and radiated sound power.

Spectral Characteristics

Figure 5 (a) and (b) show sample sound pressure level spectra measured at elevation angles of 0° and -45°, respectively, which corresponds to the two edges of the array. These two elevation angles generally bound the measured response. The noise floor in the anechoic chamber is shown by the dashed black lines. Results for the motor and drivetrain, with no rotors installed, are also shown for comparison purposes. The acoustic spectra for the single rotor, shown by the solid red lines, are dominated by tones at low frequencies. The peak at 170 Hz corresponds to the blade passage frequency. It is worth noting that noise at the blade passage frequency is more than 20 dB above the level measured with the motor and drivetrain alone. In addition to the blade passage frequency, a much lower amplitude peak is present at the second harmonic, 340 Hz. Strong tones, particularly out of the plane of the rotor, can also be seen at the rotor shaft rotation rate, 85 Hz, and at odd multiples of that frequency. The prominence of these

tones could be indicative of blade imbalance or shaft misalignment. At frequencies above 400 Hz, the motor and drivetrain tends to dominate the response. Several tones can be attributed to the motor, including 510 Hz, but the drive belts are also a significant contributor in this frequency range.
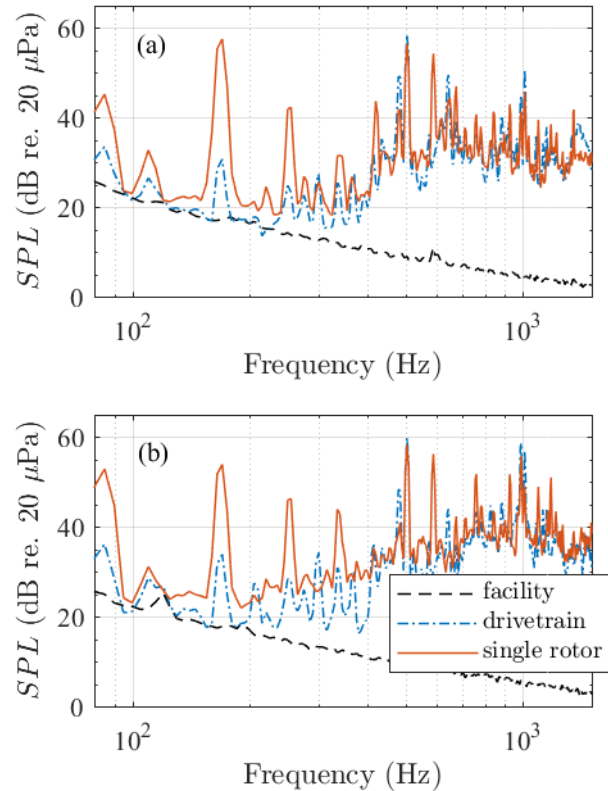

Figure 5. Sound pressure level spectra measured at elevation angles of (a) 0° and (b) -45°, corresponding to microphones M1 and M5, respectively.

During the test, several sets of measurements were collected to assess repeatability. While the typical variation observed in the tonal level at the blade passage frequency was 0.5 dB or less, it was not unusual to see 3 dB variation in the level at the second harmonic. This is consistent with previous work, which has shown that inflow distortion, due to recirculation for instance, affects the amplitude of the higher harmonics more than the fundamental (Ref. 8). Because of the low relative amplitude of the second harmonic and increased sensitivity to inflow distortion, this dataset is not well suited to evaluate changes in the amplitude of the higher harmonics due to phase control.

Source Directivity and Mean Thrust

The measured and predicted thrust are compared in Table 2. As expected, the predicted thrust for the isolated rotor is higher than measurements. In this case, the prediction is approximately 11% higher. Recall that the dual rotor assembly has a 13 mm diameter support arm beneath each rotor. The downwash on the support arm will reduce the thrust of the system relative to an isolated rotor, and could at least

5

partially explain the discrepancy. In general, however, the level of agreement for the single rotor case is acceptable. Predictions for the dual rotor configurations were generated by combining the thrust from two isolated rotors. Therefore, all five dual rotor predictions are identical. There is some variation in the measured values, particularly for the first counterrotating test. In this case, a small thrust deficit was measured. In general, however, it appears that the second rotor increases the thrust by a factor of two, regardless of the rotation direction or relative phase angle.

Table 2. Comparison of measured and predicted mean thrust.

Configuration	Measured thrust* (N)	Predicted thrust (N)
single	4.9	5.5
counterrotating, $\psi_r = 0°$	9.3	10.9
counterrotating, $\psi_r = 90°$	9.8	10.9
corotating, $\psi_r = 0°$	10.0	10.9
corotating, $\psi_r = 45°$	10.0	10.9
corotating, $\psi_r = 90°$	10.0	10.9

*Load cell bias uncertainty: ± 0.2 N

The measured and predicted in-plane (i.e., elevation angle of 0°) source directivity at the blade passage frequency are shown in Figure 6. A similar set of out-of-plane (i.e., elevation angle of -45°) source directivity plots are also included in Figure 7. These two sets of plots document the best and worst comparisons between predictions and measurements. In general, there appears to be more scatter in the measurements below the plane of the rotor, however, the azimuthal patterns tend to be consistent. The first polar plot corresponds to a single rotor, and as expected, the directivity pattern is relatively uniform. A clover-leaf pattern appears when the rotors are counterrotating, which resembles a lateral quadrupole source with 4 lobes and nulls around the azimuth. Changing the relative phase by 90° rotates the pattern, but does not have any other apparent effect on shape or amplitude. The relative phase has a more significant impact when the rotors are corotating. When the rotors are corotating, and the relative phase offset is 0°, the directivity is nearly axisymmetric, particularly in the plane of the rotor. In contrast, when the phase offset is 45°, a cardioid pattern is generated with increased radiation toward azimuthal angles of 90°. Finally, when the relative phase offset is 90°, a figure-8 pattern is produced with two lobes separated by deep nulls at 0° and 180°. This is a classic dipole radiation pattern. Aside from the change in shape, however, there is also a significant reduction in the overall amplitude, even in directions of peak radiation. This is particularly apparent below the plane of the rotor where the reduction is most pronounced. In general, the numerical model appears to capture the relevant source characteristics, including changes in both the shape and the amplitude of the radiation patterns.

(a) single

(b) cntr, $\psi_r = 0°$

(c) cntr, $\psi_r = 90°$

(d) co, $\psi_r = 0°$

(e) co, $\psi_r = 45°$
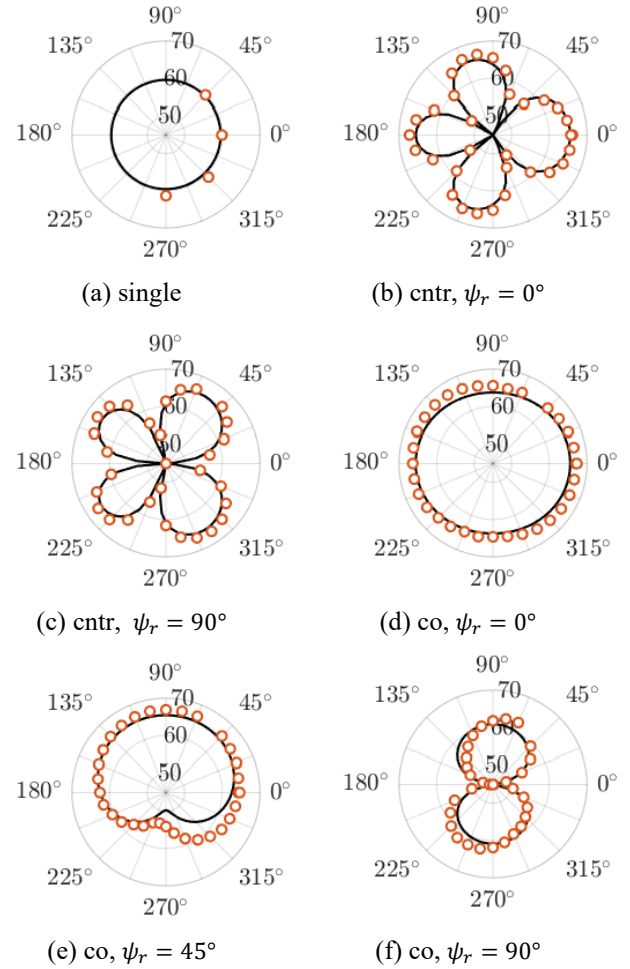
(f) co, $\psi_r = 90°$

Figure 6. Comparison of the predicted (solid black lines) and measured (red circles) sound pressure level in dB at the blade passage frequency at an elevation angle of 0°.

6

(a) single

(b) cntr, $\psi_r = 0°$

(c) cntr, $\psi_r = 90°$

(d) co, $\psi_r = 0°$
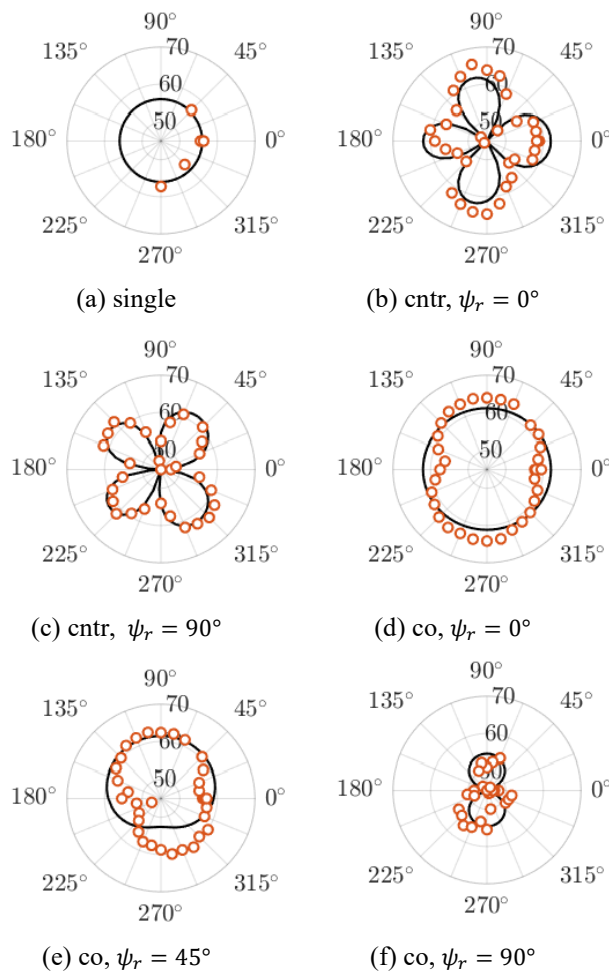
(e) co, $\psi_r = 45°$

(f) co, $\psi_r = 90°$

Figure 7. Comparison of the predicted (solid black lines) and measured (red circles) sound pressure level in dB at the blade passage frequency at an elevation angle of -45°.

Assessment of the Farfield Approximation

While the primary goal of the experiment was to collect data that could be used to assess the accuracy of the numerical model, the experimental data can also be used to directly quantify the change in radiated sound power if the microphones are in the farfield. In the farfield, pressure and particle velocity are nearly in phase, and therefore, intensity can be estimated based on pressure measurements. The intensity will also be radially directed and pressure will decay proportional to $1/r$, where r is the separation distance from the source. This final relationship is often used to identify the transition between the nearfield and farfield regions. While there are rules of thumb for identifying the boundary between these two regions, the actual location depends on the characteristics of the source and angle of the observer. A pulsating sphere that is very large relative to the acoustic wavelength, for instance, has no nearfield (Ref. 13), while farfield approximations for a baffled piston, along the piston centerline, are only accurate if the separation distance is greater than approximately seven piston radii (Ref. 14).

Previous experimental and analytical studies have evaluated the spatial decay as a function of separation distance for isolated propellers (Refs. 15, 16) and groups of unsynchronized rotors (Ref. 17). However, the authors are not aware of similar studies conducted with pairs of synchronized rotors. Since the boundary between the nearfield and farfield depends on the characteristics of the source, and the characteristics of synchronized rotors are different than isolated rotors, a numerical study was conducted to estimate the location of the boundary for the specific configurations considered in this study. Figure 6 and Figure 7 have already shown that the numerical model captures the relevant source characteristics. Therefore, the same model can be used to perform this study. Specifically, pressure was predicted along several lines extending out from the center of the two rotor system at different azimuthal and elevation angles. The sound pressure level was then plotted as a function of separation distance, along with the $20 \log_{10}(1/r)$ asymptote for comparison. The boundary between the nearfield and farfield was assumed to coincide with the location where the predicted sound pressure level converged to within 0.5 dB of the farfield asymptote.

Sound pressure level predictions for an isolated rotor at three different elevation angles are shown in Figure 8. In this case, the nearfield decay rate appears to be dependent on the elevation angle, with the in-plane response taking longest to converge. The in-plane response converges to within 0.5 dB of the farfield asymptote at a separation distance of 1.5 m, which is approximately 10 times the rotor radius.
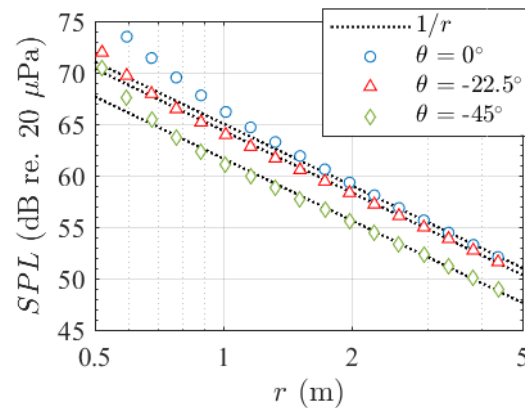

Figure 8. Sound pressure level decay at the blade passage frequency compared to the farfield inverse law (1/r) for an isolated rotor.

Figure 9 shows sound pressure level predictions, along with the $20 \log_{10}(1/r)$ asymptotes for several pairs of synchronized rotors. The in-plane response is shown, since it tends to have the slowest decay, and the azimuthal angle is 90°. In general, for sources with significant azimuthal variation, the decay rate should be evaluated at multiple azimuthal angles. However, since the ultimate goal of this assessment is to determine if the pressure measurements can be used to estimate radiated power, and power is controlled,

7

to a large extent, by the regions with the highest amplitude, it is most important to establish the validity of the farfield assumption in directions of peak radiation (i.e., maximums in the source directivity). All three configurations included in Figure 9 have a peak in the radiation pattern around 90°. For these cases, the response converges to within 0.5 dB of the farfield asymptote at a separation distance of approximately 1.75 m. While these results are typical of most angles, convergence is slower near the nulls in the directivity plots. For example, Figure 10 shows sound pressure level predictions along a line, at a 0° azimuthal angle, extending out from a pair of counterrotating rotors with a relative phase offset 90°. This angle corresponds to a null in the radiation pattern, as seen in Figure 6 (c). At this particular angle, the response still has not converged to the farfield asymptote after 5 m. Note however, that the limits on the y-axis are 20 dB lower than in previous plots, so the overall levels are relatively small. While this behavior may be an artifact of the near perfect cancellation possible in a model, it is still useful to keep in mind when comparing measured and predicted levels near the nulls in the radiation pattern. Once again, since the goal of this study is to quantify radiated power, the absolute levels in the nulls are largely irrelevant.
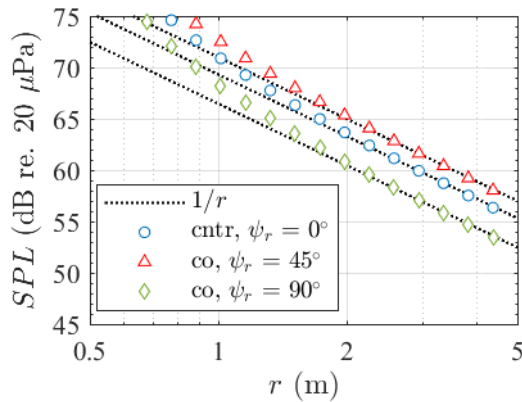

Figure 9. Sound pressure level decay at the blade passage frequency compared to the farfield inverse law (1/r) for two synchronized rotors.

To conclude, the results of the numerical study indicate that at most angles, the farfield approximation is valid at an observer distance greater than approximately 1.75 m. Recall that the microphones used in this test were located 1.9 m from the center of the assembly. Therefore, the farfield approximation should be valid at most measurement locations.
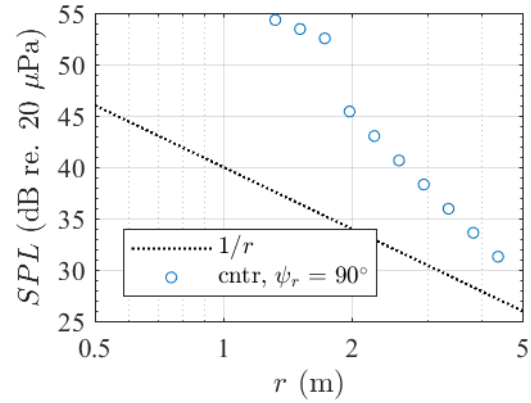

Figure 10. Sound pressure level decay compared to the farfield inverse law (1/r) in the direction of a null in the source directivity.

Radiated Sound Power

Acoustic intensity was calculated from the pressure measurements, and then radiated sound power was found by integrating the intensity over the surface area of the measurement grid, as described in the methodology section. Sound power predictions were generated in a similar way, however, the integration was either performed over a full hemisphere below the plane of the rotors, or over a full sphere surrounding the rotors. To account for differences in the integration area, the sound power was normalized by the single rotor results. This removed the area dependence and enabled a more direct comparison between measurements and predictions. Specifically, since the goal is to compare dual rotor results, the data was normalized by two times the power radiated from a single rotor. This "baseline" corresponds to the sound power radiated from two unsynchronized rotors.

Measurements and predictions of the normalized sound power are compared in Table 3. Once again, based on the way the data is normalized, the PWL for a single rotor is, by definition, -3 dB, or 3 dB less than the baseline. The dual rotor results are more interesting. First, notice that the same trends can be seen in the measurements and in both sets of predictions. For example, when the rotors are counterrotating, the radiated power is approximately equal to the reference case (i.e., close to 0 dB), regardless of the relative phase angle. This does not, however, imply that the directivity is equal. Recall from Figure 6 that synchronized, counterrotating rotors produce a strong interference pattern that depends on the relative phase angle. The fact that the overall power does not change implies that attenuation in one direction results in amplification in other directions. In contrast, when the rotors are corotating, significant changes in the overall radiated power are observed both experimentally and numerically. For example, when the relative phase offset is 0°, the radiated sound power is increased by more than 2 dB relative to the baseline. In contrast, the net change in power is negligible when the two rotors are offset by 45°. When the rotors are corotating, with a relative phase offset of 90°, both measurements and predictions show a 5-6 dB reduction in radiated power. This

suggests that phase synchronization can be used to achieve a net reduction in the acoustic energy radiated at the blade passage frequency.

Table 3. Radiated power, at the blade passage frequency, relative to 2x the power of a single rotor.

Configuration	Measured ΔPWL, hemisphere* (dB)	Predicted ΔPWL, hemisphere (dB)	Predicted ΔPWL, sphere (dB)
single	-3.0	-3.0	-3.0
cntr, $\psi_r = 0°$	0.4	0.2	-0.1
cntr, $\psi_r = 90°$	-0.3	-0.1	0.1
co, $\psi_r = 0°$	2.5	2.3	2.3
co, $\psi_r = 45°$	-0.2	-0.1	0
co, $\psi_r = 90°$	-5.8	-5.2	-5.3

*Measurements were acquired on a portion of the lower hemisphere spanning elevation angles from 0° to -45°.

Once again, since the numerical model captures the relevant trends, it can be used to more fully explore the design space. Predictions were generated for other relative phase angles. The normalized sound power calculated on the lower hemisphere is plotted in Figure 11. The two curves correspond to the predictions for the corotating and counterrotating configurations. It is clear that the relative phase offset has much more impact on the net radiated power when the rotors are corotating. In this case, there is a global minimum at a relative phase offset of 90°, corresponding to a reduction of 5.2 dB. In contrast, the maximum change in power is less than 0.2 dB when the rotors are counterrotating. The measured values are also included in the figure for comparison purposes.
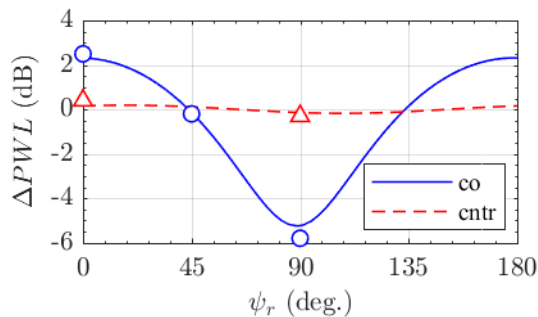

Figure 11. Normalized sound power radiated from a pair of 2-bladed synchronized rotors with a kd of 1.2. Measured values are indicated with markers.

While the relative phase offset is an important parameter affecting radiated power, other parameters are expected to have an impact as well. For example, previous work has shown that kd has a significant impact on the directivity pattern produced by a pair of synchronized propellers (Ref. 4). In this context, k is the acoustic wavenumber and d is the hub to hub separation distance. This parameter is sometimes called the compactness ratio since it quantifies the size of the source relative to the acoustic wavelength. For the tests conducted within this study, kd equals 1.2 at the blade passage frequency. To assess the impact of this parameter, a parametric sweep was performed over kd values from 0.1 to 10 and relative phase angles, ψ_r, from 0° to 180°. Predictions, in the form of contour plots, are given in Figure 12. The colors represent normalized sound power radiated below the plane of the rotors, relative to two unsynchronized rotors. Figure 12 (a) corresponds to two synchronized counterrotating rotors, and Figure 12 (b) corresponds to two corotating rotors. Each contour line represents a change of 0.5 dB. As previously observed, the largest changes occur when the rotors are corotating. In this case, there are multiple local minimum; however, the largest reduction occurs at low kd values when the relative phase offset is 90°. In other words, to achieve the maximum reduction in radiated power using corotating rotors, the separation distance between the rotors needs to be small relative to the acoustic wavelength. In general, this trend makes sense. As the separation distance between the rotors gets small relative to the acoustic wavelength, the pair of 2-bladed rotors will radiate like a single 4-bladed rotor. In other words, the pair of rotors will not radiate efficiently at two times the shaft rate, but will instead radiate most efficiently at four times the shaft rate. It therefore seems possible that the reductions at the blade passage frequency could result in higher levels at the second harmonic. Note however that the kd value at the second harmonic is two times higher. Based on the trends in Figure 12 (b), the change in power at the second harmonic should be less than the change at the fundamental. Therefore, any increase in power at higher harmonics, due to phase control, is expected to be modest. Recall that the current data set is not ideally suited to evaluate changes in the amplitude of the higher harmonics. Therefore, this effect could not be evaluated experimentally.

The overall trend is quite different when the rotors are counterrotating, as shown in Figure 12 (a). In this case, maximum attenuation occurs at a kd value of 5.8, which is approximately when the separation distance equals the acoustic wavelength. While the potential benefit is smaller, on the order of 2 dB, this condition may be easier to achieve on some vehicles, and is therefore worth further investigation. Differences between the corotating and counterrotating configurations, particularly with respect to kd, suggest that different physical mechanisms may be responsible for the observed changes in radiated power.
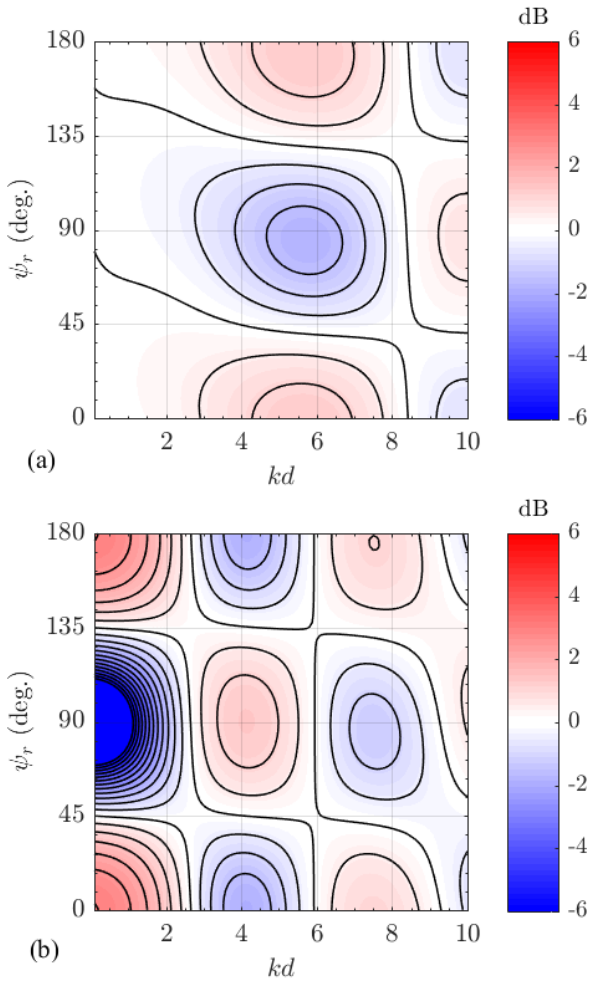
Figure 12. Normalized sound power contours for a pair of (a) counterrotating and (b) corotating rotors.

It is important to note that the predictions presented in this paper are applicable to 2-bladed rotors. The optimal relative phase angle will vary based on the blade count. For example, the optimal relative phase offset is expected to be 60° for a 3-bladed rotor and 45° for a 4-bladed rotor. The blade passage frequency, however, is also proportional to the blade count. Therefore, for a fixed rotation rate and rotor layout, kd will increase proportional to the blade count. This means the overall potential benefit, in terms of sound power, will also be affected by blade count.

Physical Explanation

While a physical explanation for the observed change in radiated power is proposed for the configuration with corotating rotors, a different explanation, not provided in this paper, is necessary to explain the trends observed for the counterrotating pair. One explanation for the change in power from the corotating rotors is that the nearfield acoustic interaction changes the radiation efficiency, and therefore net radiated power of the two rotor system. This is a common explanation in other areas of acoustics. For example, a dipole, which consists of two closely spaced monopoles with the same source strength but opposite phase, radiates less efficiently than a single monopole. When the two monopoles are close together, the pressure field of one source modifies the power output of the second source, and vice versa. This interaction does not change the source strength of either monopole, but instead modifies the radiation efficiency of each source (i.e., affects how efficiently the mechanical energy is converted to acoustic energy) (Ref. 18). The separation distance between the sources is important however. As the separation distance is increased relative to the acoustic wavelength, the ratio of the sound power output of a dipole relative to a monopole asymptotes to 2 (i.e., +3 dB). In other words, at large separation distances, the power output of the dipole is twice as much as the monopole, which is an intuitive result for two non-interacting acoustic sources. To compare with the rotor predictions, the change in radiated power for the dipole is plotted in Figure 13 with respect to the power radiated by two incoherent monopoles. This can be calculated as $\Delta PWL = 1 - (\sin kd)/kd$ (Ref. 18). The normalized power for two corotating rotors with a relative phase offset of 90° is also shown as a function of kd, along with the corresponding measurement (at a kd of 1.2). The strong similarity between the curves suggests that similar physical mechanisms may explain both trends. Note that in both cases, the separation distance needs to be much less than half the acoustic wavelength (i.e., $kd \ll \pi$) to get significant attenuation.
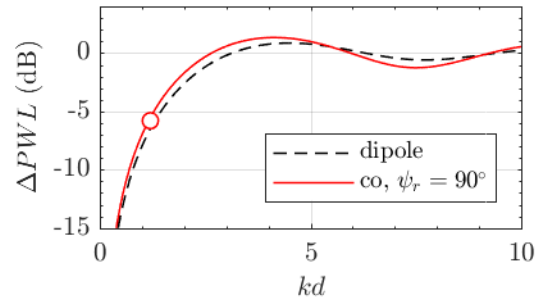

Figure 13. Normalized sound power radiated from a dipole compared to two corotating rotors with a relative phase offset of 90°. The corresponding measured value for corotating rotors is indicated by the circle.

Potential Vehicle Level Benefit

The potential vehicle level benefit is evaluated by comparing ground contours beneath an octocopter. For this evaluation, the vehicle is assumed to be 10 m above the ground plane, hovering with either eight unsynchronized rotors, or four pairs of synchronized corotating rotors. In the second case, the relative phase angle between rotors within each pair is assumed to be 90°. Recall that each pair of rotors is assumed to match the operating conditions and geometry of the test assembly. A comparison between the two operating conditions, in terms of the sound pressure level at the blade passage frequency on the ground, is shown in Figure 14. Figure 14 (a) corresponds to the baseline case with eight unsynchronized rotors, while Figure 14 (b) shows the benefit

of synchronizing, and fixing the relative phase between pairs of rotors. As previously shown, the sound power radiated from the pair of synchronized, corotating rotors is approximately 5 dB less than the power radiated from a similar pair of unsynchronized rotors. A 5 dB reduction from each pair of rotors will in turn reduce the total vehicle level sound power by 5 dB. For this particular example, phase synchronization leads to a global reduction of the sound pressure level at the blade passage frequency on the ground plane. Specifically, the level is reduced by 4-5 dB nearly everywhere with peak reductions of approximately 6 dB near the vehicle.
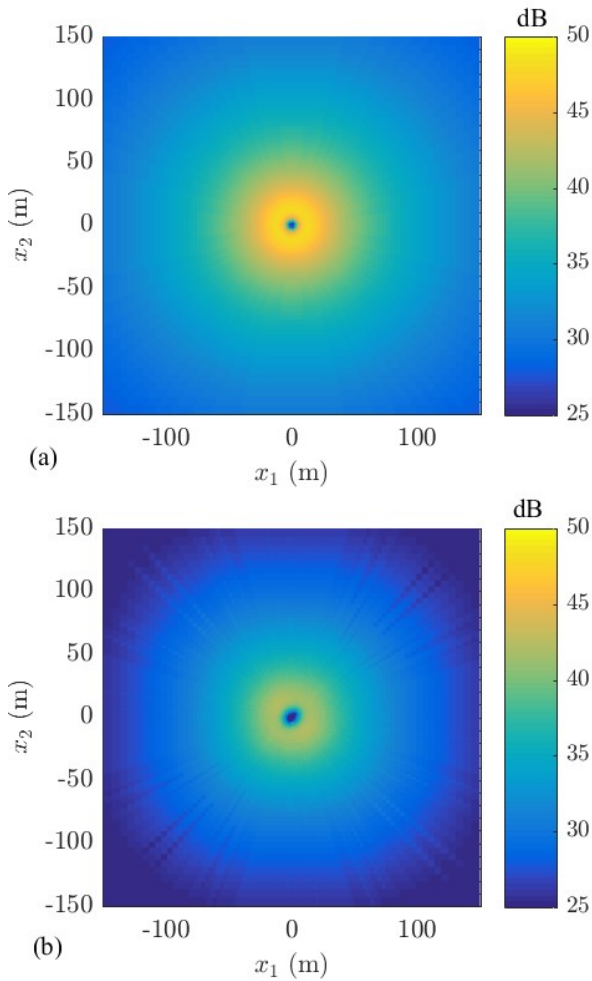

(a)

(b)

Figure 14. Predicted sound pressure level at the blade passage frequency below a small octocopter with (a) unsynchronized rotors or (b) pairs of synchronized rotors with a relative phase offset of 90°.

CONCLUDING REMARKS

The purpose of this study was to determine if phase synchronization could be used to achieve an overall reduction of the sound power radiated by two rotors. The study included both experimental and numerical components. Results from the experiments confirmed that the model accurately captures the sound radiation from two synchronized rotors. The model

was then used to explore the design space and evaluate the potential vehicle level benefit of using phase synchronization with pairs of matched rotors. Specific findings of the study include:

- Both measurements and predictions show that the radiated sound power at the blade passage frequency can be reduced by synchronizing and controlling the relative phase of two rotors. A reduction of over 5 dB was achieved experimentally with no thrust impact.
- The optimal relative phase offset for 2-bladed rotors is 90°.
- Corotating rotors provide more potential benefit than counterrotating rotors.
- For corotating rotors, the maximum benefit is achieved when the separation distance between the rotors is small relative to the acoustic wavelength. Specifically, the separation distance needs to be much less than half the acoustic wavelength to get significant attenuation.
- Numerical predictions show that the maximum benefit for counterrotating rotors is achieved when the separation distance between rotors is approximately equal to the acoustic wavelength (i.e., $kd \approx 2\pi$).
- The vehicle level benefit was predicted for an octocopter in hover. At the operating conditions considered, a 5 dB reduction in source power, due to phase synchronization, resulted in a 4-5 dB reduction in the SPL at the blade passage frequency nearly everywhere on the ground plane.

In conclusion, this study demonstrated that phase synchronization, with matched rotor pairs, could be used to reduce the average noise radiated from a vehicle at the blade passage frequency. The study, however, was restricted to relatively small rotors with uniform inflow. Before synchronization is applied to something like an octocopter, the benefits need to be assessed in edgewise flight. Additional work is also needed to determine if phase synchronization affects the acoustic energy at the higher harmonics. The predicted change in sound power at high kd values for counterrotating rotors needs to be confirmed experimentally. This configuration is particularly interesting because it could be applied to a larger class of vehicles. Follow-on activities could also assess the benefit of synchronizing sets of propellers, potentially more than two, in forward flight. Since two corotating, out-of-phase rotors behave similar to an acoustic dipole, it may be possible to use 4 propellers, synchronized and phased appropriately, to mimic an acoustic quadrupole, which radiates even less efficiently than a dipole.

Author contact: Noah Schiller noah.h.schiller@nasa.gov, Kyle Pascioni kyle.a.pascioni@nasa.gov, Nikolas Zawodny nikolas.s.zawodny@nasa.gov

ACKNOWLEDGMENTS

Advanced Air Vehicles Program, for this study.

REFERENCES

1. Silva, C., Johnson, W., Antcliff, K. R., and Patterson, M. D., "VTOL urban air mobility concept vehicles for technology development," Paper AIAA 2018–3847, 2018 Aviation Technology, Integration, and Operations Conference Proceedings, Atlanta, GA, 2018.
2. Pascioni, K. A., and Rizzi, S. A., "Tonal noise prediction of an unmanned aerial vehicle," Paper AIAA 2018-2951, 24th AIAA/CEAS Aeroacoustics Conference Proceedings, Atlanta, GA, June 25-29, 2018.
3. Pascioni, K. A., and Rizzi, S. A., "Auralization of an unmanned aerial vehicle under propeller phase control," InterNoise 2018 Proceedings, Chicago, IL, August 26-29, 2018.
4. Pascioni, K. A., Rizzi, S. A., and Schiller, N.H., "Noise reduction potential of phase control for distributed propulsion vehicles," Paper AIAA 2019-1069, AIAA SciTech Forum and Exposition Proceedings, San Diego, CA, January 2019.
5. Zawodny, N.S., and Boyd, D.D., "Investigation of rotor-airframe interaction noise associated with small-scale rotary-wing unmanned aircraft systems," American Helicopter Society 73rd Annual Forum Proceedings, Ft. Worth, TX, May 2017.
6. Patterson, A., Gahlawat, A., and Hovakimyan, N., "Propeller phase synchronization for small distributed electric vehicles," Paper AIAA 2019-1458, AIAA SciTech Forum and Exposition Proceedings, San Diego, CA, January 2019.
7. Grosveld, F. W., "Calibration of the Structural Acoustics Loads and Transmission Facility at NASA Langley Research Center," InterNoise 99 Proceedings, Ft. Lauderdale, FL, Dec.6-8, 1999.
8. Stephenson, J.H., Weitsman, D., and Zawodny, N.S., "Effects of flow recirculation on unmanned aircraft system (UAS) acoustic measurements in closed anechoic chambers." *Journal of the Acoustical Society of America*, Vol. 145, (3), 2019, pp. 1153-1155.
9. Nguyen, L. C., and Kelly, J. J., "A users guide for the NASA ANOPP Propeller Analysis System", NASA CR 4768, 1997.
10. Zorumski, W., "Aircraft Noise Prediction Program theoretical manual, Part 1," NASA TM-93199, 1982.
11. Zawodny, N., Boyd, D., and Burley, C., "Acoustic characterization and prediction of representative, small-scale rotary-wing unmanned aircraft systems components," American Helicopter Society 72nd Annual Forum, West Palm Beach, FL, May 2016.
12. Farassat, F., "Theory of noise generation from moving bodies with an application to helicopter rotors," NASA TR-R-451, 1975.
13. Bies, D. A, and Hansen, C. H., *Engineering Noise Control*, E & FN Spon, London, 1996, pp. 198.
14. Kinsler, L. E., Frey, A. R., Coppens, A. B., and Sanders, J. V., *Fundamentals of Acoustics, 4th edition*, John Wiley & Sons, 2000, pp. 179-181.
15. Turkdogru, N., and Ahuja, K.K., "Determination of geometric farfield for ducted and unducted rotors," *International Journal of Aeroacoustics*, Vol. 11, (5&6), 2012, pp. 607-628.
16. Ianniello, S., "The Ffowcs Williams-Hawkings equation for hydroacoustic analysis of rotating blades. Part 1. The rotpole," *J. Fluid Mech.*, Vol. 797, 2016, pp. 345-388.
17. Tinney, C.E., and Sirohi, J., "Multirotor drone noise at static thrust," *AIAA Journal*, Vol. 56, (7), 2018, pp. 2816-2826.
18. Nelson, P.A., Curtis, A.R.D., Elliott, S.J., and Bullmore, A.J., "The minimum power output of free field point sources and the active control of sound," *J. of Sound and Vibration*, Vol. 116, (3), 1987, pp. 397-414.